Journal of Nanobiotechnology

RESEARCH Open Access

Dual targeting and bioresponsive nano-PROTAC induced precise and effective lung cancer therapy

Xiaoling Guan[1†], Xiaowei Xu[1†], Yiwen Tao[1†], Xiaohua Deng[1], Linlong He[1], Zhongxiao Lin[1], Jishuo Chang[1], Jionghua Huang[2], Dazhi Zhou[3], Xiyong Yu[1,3*], Minyan Wei[1,3*] and Lingmin Zhang[1,3*]

Abstract

Epigenetic regulation has emerged as a promising therapeutic strategy for lung cancer treatment, which can facilitate the antitumor responses by modulating epigenetic dysregulation of target proteins in lung cancer. The proteolysis-targeting chimera (PROTAC) reagent, dBET6 shows effective inhibition of bromodomain-containing protein 4 (BRD4) that exerts antitumor efficacy by degrading BRD4 via the ubiquitin-proteasome system. Nevertheless, the low tissue specificity and bioavailability impede its therapeutic effects and clinical translation on lung cancer treatment. Herein, we developed a type of dual targeting and bioresponsive nano-PROTAC (c *R* GD/*L* LC membrane/*D* S-*P* LGA/d *B* ET6, named RLDPB), which was constructed by using the pH and glutathione (GSH)-responsive polymer, disulfide bond-linked poly(lactic-co-glycolic acid) (PLGA-S-S-PLGA, DS-PLGA) to load the PROTAC agent dBET6, and further camouflaged with the homotypic LLC cell membranes, followed by the conjugation with cRGD ligand to the surface of the nanoparticles. Notably, RLDPB showed enhanced celluar uptake by lung cancer cells in vitro and accumulation in the tumors via the dual targeting structure including cRGD and LLC membrane. The pH/GSH responsiveness improved the release of dBET6 from the DS-PLGA-based nanoparticles within the cells. RLDPB was demonstrated to facilitate tumor regression by inducing the apoptosis of lung cancer cells with the degradation of BRD4. Thus, RLDPB can be considered a powerful tool to suppress lung cancer, which opens a new avenue to treat lung cancer by PROTAC.

Introduction

Lung cancer is one of the most prevalent malignancy tumors and the leading cause of cancer-related death in the globe, which accounts for approximately 2 million new incidences and 1.76 million deaths annually [1]. Patients who suffer from lung cancer receive clinical treatments with surgery, chemotherapy, radiotherapy, immunotherapy, or the multimodal combination of these therapies mentioned above [2, 3] However, the present approaches showed limited therapeutic effects on lung cancer [4]. Thus, novel strategies for precisely eliminating tumors are demanded in lung cancer treatment.

†Xiaoling Guan, Xiaowei Xu and Yiwen Tao contributed equally to this work.

*Correspondence:
Xiyong Yu
yuxycn@aliyun.com
Minyan Wei
weiminyan@163.com
Lingmin Zhang
zhanglm@gzhmu.edu.cn

Full list of author information is available at the end of the article

Graphical abstract

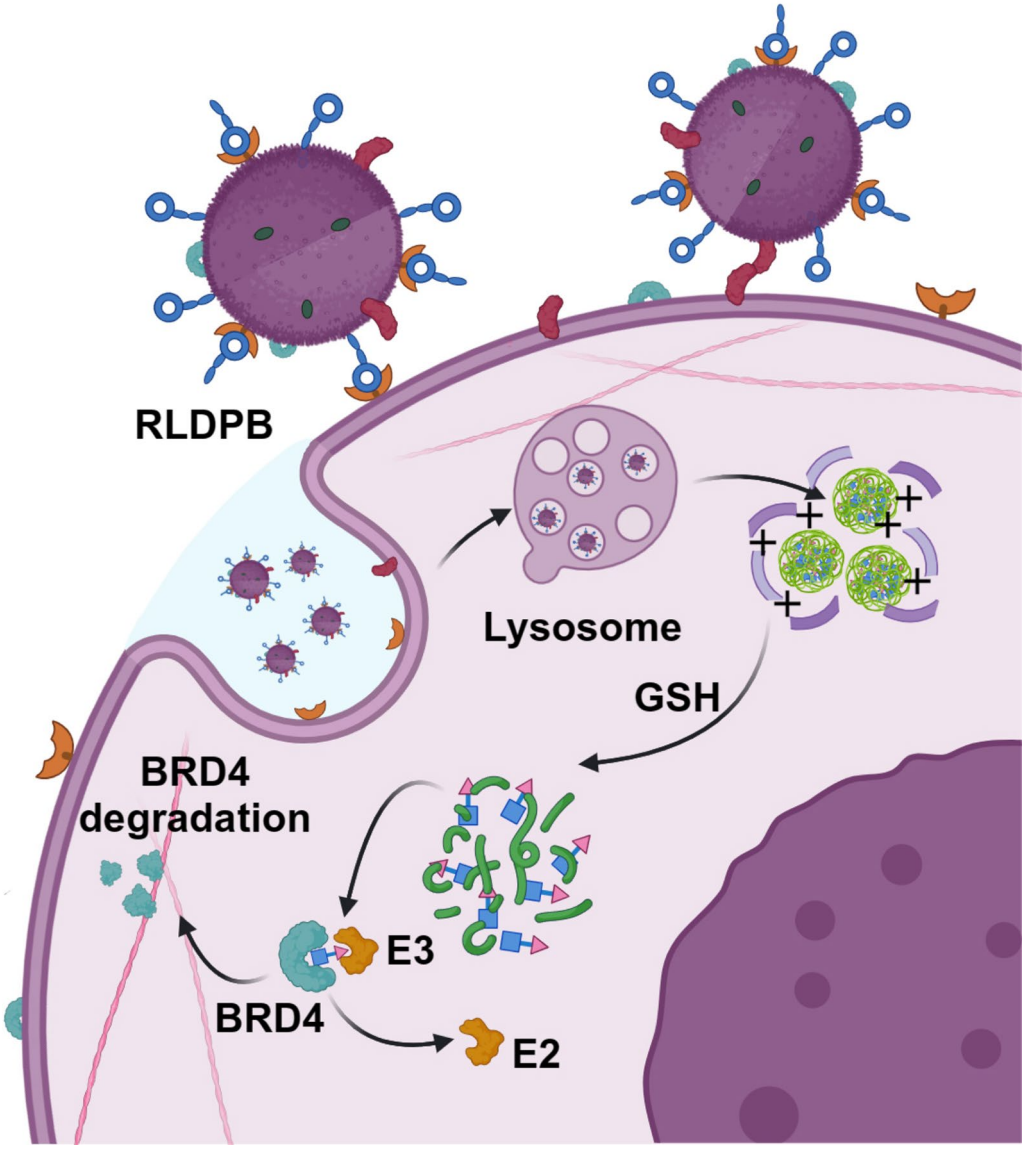

Keywords PROTAC, dBET6, Dual targeting, Bioresponsiveness, Lung cancer

Epigenetic regulation has emerged as a promising therapeutic strategy for cancer treatment, in which epigenetic drugs can facilitate the antitumor responses by modulating the target protein or gene expression in tumors with epigenetic dysregulation [5, 6]. Genome-wide studies of lung cancer reveal that bromodomain-containing protein 4 (BRD4), one of the epigenetic reader proteins in the bromo- and extra-terminal domain (BET) motif family, exhibits apparent epigenetic dysregulation and promotes tumor growth in lung cancer. Importantly, the BRD4 inhibitions lead to tumor regressions by inducing cell apoptosis through the Caspase-3 pathway, highlighting that BRD4 is the potential target for lung cancer therapy [7]. So far, various BET inhibitors such as JQ1 and I-BET762 (GSK525762, Molibresib), have been demonstrated to show antitumor effects in early clinical development [8]. Nevertheless, the low tissue specificity and acquired BETi resistance limit their applications in cancer therapy [9]. More effective BET regulators are in great demand for lung cancer therapy.

Proteolysis-targeting chimera (termed PROTAC) has become an effective tool to degrade the targeted protein, which exerts a powerful effect on cancer therapy [10, 11]. Recently, dBET6, a PROTAC reagent of BRD4, has been

proven to effectively eliminate lung cancers by inducing cell apoptosis with the targeted degradation of BRD4 [12]. However, the low tissue specificity and bioavailability obstructed its clinical translation on lung cancer treatment. Improving the specificity and bioavailability of dBET6 may contribute to facilitating lung cancer therapy. Various approaches have been developed to carry the PROTAC regents. Ping et al. developed a bioorthogonal PROTAC prodrug capable of degrading the target protein and treating the tumor precisely [13]. Sheng et al. synthesized a drugtamer-PROTAC conjugation to enhance tumor targeting and antitumor potency [14]. Li et al. introduced a ClickRNA-PROTAC system, which selectively degraded proteins of interest in tumor cells [15]. Nanotechnology was also used to construct the PROTAC formulations. Yu et al. presented the polymeric PROTAC (POLY-PROTAC) nanotherapeutics for tumor-specific protein degradation [16]. Pu et al. developed a semiconducting polymer nano-PROTAC with phototherapeutic and activatable protein degradation abilities for photoimmunometabolic cancer therapy [17]. Su et al. used cationic liposomes to co-deliver PROTAC and siRNA to attain enhanced protein clearance efficiency and tumor therapeutic effects [18]. These studies represented the latest progress in PROTAC delivery, which contributed to the potential clinical applications. To further improve the therapeutic effects, the surface properties and the drug release should be focused on, for the factors are closely related to whether the drug can achieve the lesion sites and run out from the vehicles, which determines the drug availability directly.

Biomimetic technology is a revolutionized approach to improve the surface function of nanoparticles [19–21]. Ascribed to the endowed functions by the biomimetic structure, the nanoparticles showed enhanced accumulation in the tumor sites with prolonged circulation and selective delivery to the tumor, which improved the therapeutic effects and inhibited tumor growth effectively [22–24]. To further improve the specific delivery of cargo, the modification by targeting ligands on the biomimetic nanoparticles is a convenient and effective approach [25]. The short peptide cyclo-arginine-glycine-aspartic acid (cRGD) is a targeting ligand binding to a_vb_3 integrin protein expressed in lung cancer, which has been successfully applied to achieve enhanced antitumor effect for lung cancer targeting treatment [26]. However, the direct conjugation with cRGD on the surface of the lung cell membrane is challenged by the potential auto-agglutination induced by the binding between cRGD and a_vb_3 on the surface of biomimetic nanoparticles. Approaches such as RNAi or knockout of a_vb_3 by gene editing suffer from a complicated process and may lead to cell death, which increases the difficulties in collecting cell membranes on a large scale. Thus, the solution on this issue may endow the nanoparticles with dual targeting capability and improved stability.

The release efficiency is another important parameter for the effective lung cancer therapy. Although dBET6 shows powerful degradation effects on BRD4, its intracellular release is usually limited to the biodegradation of the vehicles. The Food and Drug Administration-approved polymer, poly(lactic-co-glycolic acid (PLGA) shows excellent performance in drug delivery, based on the characteristics such as high loading efficiency, high biosafety, and biodegradation. However, previous work indicated that PLGA-based nanoparticles suffered from partial degradation within the endo/lysosomes, and a large amount of intact or damaged nanoparticles may escape in the process of endosomal recycling [27, 28]. The behaviors may greatly impede the cargo release intracellularly and reduce the therapeutic effects, especially for the challenged diseases including cancer. Our previous work indicated that the pH and glutathione (GSH)-responsive polymer, disulfide bond-linked poly(lactic-co-glycolic acid) (PLGA-S-S-PLGA, DS-PLGA) was endowed with enhanced properties in the responsive release of PROTAC regents, which showed great potential in drug delivery [29].

In the present work, a type of dual targeting and bioresponsive nano-PROTAC (named RLDPB) was developed to induce the degradation of BRD4 in lung cancer cells, which was expected to improve the precise treatment of lung cancer. The nano-PROTAC was constructed by the use of pH/Glutathione (GSH)-responsive polymer (PLGA-S-S-PLGA, DS-PLGA) to load the PROTAC agent dBET6 as a core, and further camouflage with lung cancer cell membranes. The a_vb_3 on the surface of biomimetic nanoparticles were blocked, followed by the modification with cRGD ligands on the surface (Scheme 1A). RLDPB was hypothesized to improve the specific delivery greatly due to the functions of the dual targeting effect, which was achieved by the homotypic targeting of LLC membranes and the binding with a_vb_3 integrin induced by cRGD. RLDPB triggered the stimulated release of dBET6 within the lung cancer cells endowed with the pH/GSH responsive ability of DS-PLGA, which precisely degraded BRD4, facilitating cell apoptosis, and tumor suppression in lung cancer treatment (Scheme 1B). This work developed a type of nano-PROTAC with dual targeting and bioresponsiveness, which might be considered a promising nanodrug for lung cancer therapy.

Materials and methods

Materials

The peptide conjugation, including cyclo-arginine-glycine-aspartic acid-polyethylene glycol (cRGD-PEG) and cyclo-arginine-glycine-aspartic acid-polyethylene glycol- 1,2-distearoyl-sn-glycero-3-phosphoethanolamine

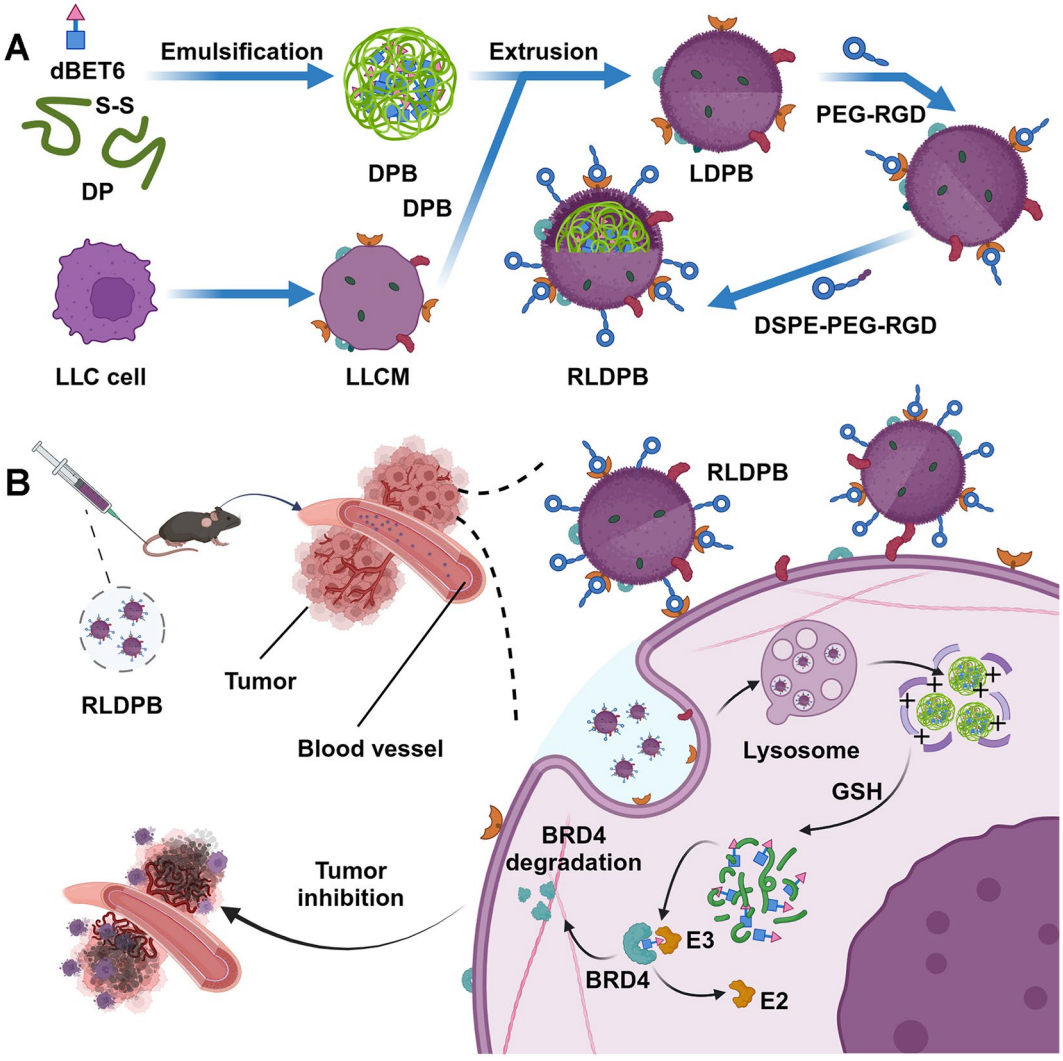

Scheme 1 Schematic illustration of the preparation of nano-PROTAC (RLDPB) and its therapeutic effects on lung cancer. (**A**) The preparation of RLDPB. (**B**) RLDPB induced therapeutic effects on lung cancer

(cRGD-PEG-DSPE) were purchased from Ruixibio (Xi'an, China). PLGA10k-S-S-PLGA10k (DS-PLGA) was also purchased from Ruixibio (Xi'an, China). dBET6 was provided by Selleck Chemicals (Houston, USA). 1,1'-dioctadecyl-3,3,3',3'-tetramethylindotricarbocyaninc iodide (DiR, purity > 98%), 1,1'-dioctadecyl-3,3,3',3'-tetramethylindodicarbocyanine perchlorate (DiD, purity > 98%), Actin tracker Red-555, Hoechst 33,342, and Annexin V-FITC/PI Apoptosis Detection kit was purchased from Thermo Fisher (Massachusetts, USA). Membrane protein extraction kit, BCA protein assay kit, cell counting kit-8 (CCK-8), Calcein-AM/PI double-stained kit and were provided by Beyotime (Jiangsu, China). Mouse Lewis lung carcinoma cells (LLC cells) were purchased from the Shanghai Institute of Cell Biology (Shanghai, China). Dulbecco's modified Eagle's medium (DMEM), fetal bovine serum (FBS), and the antibiotics penicillin-streptomycin were purchased from Hyclone (Logan, USA). C57BL/6 mice (6-week-old, 20 g weight) were purchased from SPF (Beijing) Biotechnology Co., Ltd. (Beijing, China).

Preparation of dBET6 loading DS-PLGA

dBET6-loaded DS-PLGA nanoparticles (DS-PLGA/dBET6, DPB) were prepared by the O/W emulsion method with minor modification [29]. Briefly, the polymer DS-PLGA was dissolved in ethyl acetate/dichloromethane (volume ratio of 3/7, 1 mL), and the PROTAC agent dBET6 was dissolved in dichloromethane, respectively. The dissolved DS-PLGA and dBET6 were mixed as the oil phase. Then, the oil phase was dropwise added into a 3% polyvinyl alcohol solution (PVA, weight/volume, 4 mL) under an ice bath with sonication (150 W, 5 min) to obtain the O/W emulsion. After stirring with 10 mL double-distilled water (ddH2O) at room temperature and

evaporating the organic solvent for 4 h, dBET6 loaded DS-PLGA nanoparticles (DPB) were collected by centrifugation (12 000 g, 40 min), followed by the washing with phosphate buffer saline (PBS), and finally resuspended in PBS for use.

To optimize the formulation of DPB, the nanostructure was prepared with different weight ratios of DS-PLGA to dBET6 (1, 2.5, 5, 10, 15, 20, 30, 40, and 50) by the O/W emulsion method. To track the in vitro and in vivo distribution of nanoparticles, the fluorescent dyes of DiD or DiR were selected to substitute dBET6 and prepared with 0.1% (weight/weight) of the DP.

Construction of cRGD/LLCM/DS-PLGA/dBET6 (RLDPB)

RLDPB was constructed according to the previous work with minor modifications [30]. Firstly, LLC cell membrane (LLCM) was extracted from LLC cells by the membrane protein extraction kit according to the manufacturer's protocol, followed by the quantification of cell membrane proteins by Bicinchoninic acid (BCA) assay. DPB and LLCM at different weight ratios were mixed under sonication (80 W, 5 min) on ice to obtain LLCM/DS-PLGA/dBET6 (LDPB) [31]. Afterward, the peptide conjugate, cRGD-PEG was incubated with LDPB suspensions in different cRGD-PEG/LLCM ratios (0.5:1, 1:1, 2:1, 4:1, weight ratio) for 4 h, followed by the wash with PBS thrice.

To confirm the blockage of a_vb_3 on the biomimetic nanoparticles, different formulations including DPB, LDPB, and RLDPB were incubated with the 5% BSA for 1 h, and then incubated with the a_vb_3 antibody (1:200, Abcam, USA) overnight. After washing by PBS thrice, the treated nanoparticles were incubated with the corresponding horseradish peroxidase (HRP)-conjugated secondary antibodies (antibody concentration of 1:1000, Abcam, USA) for 1 h, followed by another PBS washing thrice. Finally, the samples were imaged and detected by the chemiluminescence imaging system (GE, USA).

After confirming the blockage of a_vb_3 on the nanopartciels, cRGD-PEG-DSPE was incubated with LDPB for 4 h, followed by extruding 20 times to obtain RLDPB. Nanoparticles including RLDP, LDPB, DiD labeled nanoparticles (LDP/DiD and RLDP/DiD), and DiR labeled nanoparticles (LDP/DiR and RLDP/DiR) were also constructed by the same procedure.

To verify the successful conjugation of cRGD-PEG-DSPE to the surface of nanoparticles, the Fluorescence resonance energy transfer (FRET) analysis was performed. Briefly, the fluorescence dye Cyanine 3 (Cy3) was used to replace dBET6, and the LLCM camouflaged nanoparticles LDP/Cy3 was prepared. After the blocking with cRGD-PEG, the fluorescein isothiocyanate (FITC) labeled cRGD-PEG-DSPE (FITC-cRGD-PEG-DSPE) was added to LDP/Cy3 suspension at different weight ratios. The emission spectra were recorded at an excitation wavelength of 488 nm with an RF-6000 Fluorescence spectrophotometer (SHIMADZU, Japan).

Characterization of the constructed nanoparticles

Transmission electron microscopy (TEM, JEOL, Japan) was used to observe the morphology of DPB, LDPB, and RLDPB. The Zeta sizer Nano ZS90 instrument (Malvern, UK) was used to measure the particle size and zeta potential of DPB and RLDPB. The prepared RLDPB were suspended in the PBS, and the stability of the nanoparticles was evaluated by the particle size and zeta potential via the zeta sizer within 96 h. The nanoparticles were also characterized by sodium dodecyl sulfate-polyacrylamide gel electrophoresis (SDS-PAGE). Briefly, LLCM, DPB, LDPB, and RLDPB was lysed with Radio Immunoprecipitation Assay (RIPA) Lysis buffer. The proteins were boiled to denature, and the concentration of proteins was quantified by BCA assay. The samples with the protein concentration of 30 μg was added to the well on the SDS-PAGE gel. The protein components were detected by SDS-PAGE. The gel was stained with Coomassie brilliant for 10 min and washed to clear with PBS.

To evaluate the responsiveness of pH and GSH, RLDPB was exposed to acidic and GSH environments. Briefly, RLDPB were incubated for 72 h with various concentrations of GSH (0, 5, and 10 mM) at pH 5.5 and 7.4, respectively. After that, the morphology of RLDPB was observed with TEM (JEOL, Japan).

To measure the drug entrapment efficiency and loading efficiency by DS-PLGA, the unencapsulated dBET6 was removed by the repeated washing of PBS and then determined at 260 nm by a UV-2600i Ultraviolet-vision spectrophotometer (SHIMADZU, Japan). The entrapment efficiency and loading efficiency of these nanoparticles were calculated by the following formula:

$$\text{Entrapment efficiency}\,(\%) = [(\text{Wi} - \text{Ws})/\text{Wi}] \times 100 \quad (1)$$

$$\text{Loading efficiency}\,(\%) = [(\text{Wi} - \text{Ws})/\text{Wt}] \times 100 \quad (2)$$

Where Wi is the total weight of dBET6 initially added in the formulation, Ws is the weight of dBET6 in supernatants, and Wt is the total weight of the nanoparticles.

In vitro drug release assay

The in vitro drug release was tested by the dialysis method in acidic/GSH environments. Briefly, the RLDPB suspensions (containing 200 μg/mL dBET6, 1 mL) were placed into the dialysis bag with a molecular weight of 14 000 Da. Then, the samples were dialyzed in 15 mL of drug release medium with a shaking speed of 120 r/min at 37 °C. The phosphate buffer saline (PBS) solution (containing different GSH concentrations of 0, 5, and 10 mM,

with pH 5.5 and pH 7.0) was chosen as the drug release medium. The release medium (1 mL) was taken out at each predetermined time interval, and measured by the UV-2600i Ultraviolet-vision spectrophotometer (SHIMADZU, Japan) at 260 nm to calculate the release rate of dBET6.

Cell culture

Lewis lung carcinoma (LLC) cells were cultured in Dulbecco's modified Eagle's (DMEM) medium (Hyclone, USA) supplemented with 10% fetal bovine serum (FBS, Hyclone, USA) and 1% penicillin/streptomycin, and incubated in the humidified atmosphere with 5% CO_2 at 37 °C.

Cellular uptake

Cellular uptakes of the nanoparticles were measured by confocal laser scanning microscopy imaging (CLSM) and flow cytometry (FACS). Briefly, LLC cells (with a cell density of 2×10^5 cells per well) were seeded into the confocal dishes and incubated for 24 h. The cells were incubated with different DiD-labeled nanoparticles (nanoparticles concentration ranging from 50 μg/mL to 400 μg/mL) or predetermined time (3, 6, 9, and 12 h). After that, the treated cells were washed with PBS thrice and fixed with 4% paraformaldehyde for 15 min. Then, the cells were stained with the actin tracker red-555 for 50 min, followed by the cell nuclei staining by the Hoechst 33,342 for 15 min. Finally, the treated cells were observed by the CLSM analysis (Zeiss LSM 880, Germany). Cells without any treatments were chosen as the negative controls. Meanwhile, cells were treated and collected in the same manner for quantitative flow cytometry analysis with a Beckman EPICS XL FACS (Beckman, USA).

Hemolysis assay

The hemolysis assay was carried out to evaluate the biocompatibility of RLDPB. Briefly, the whole blood was obtained from the C57BL/6 mice with the heparin sodium treatment. The red blood cells (RBCs) were collected by centrifugation at 3000 g for 5 min, followed by thrice washing and resuspending by PBS. Then, dBET6, DPB, LDPB, and RLDPB (dBET6 equivalent to 7.5 μg/mL) were incubated in the 2% RBCs suspension (1 mL) for 1 h, followed by the centrifugation at 10,000 g for 10 min, respectively. The supernatant was determined at 540 nm by a microplate reader (Thermo, USA) to calculate the hemolysis percentage according to the following formula. Meanwhile, RBCs without any treatment served as the negative controls, and RBCs treated with 0.2% Triton X-100 were selected as the positive controls.

$$\text{Hemolysis}\,(\%) = [(\text{As} - \text{Ac})/\text{At} - \text{Ac}] \times 100\% \quad (3)$$

Where A_s stands for the absorbance of the tested samples, Ac stands for the absorbance of the negative controls, and At stands for the absorbance of Triton X-100.

Cell counting kit-8 assay

The cytotoxicity of RLDPB was investigated by the cell viability measured with the cell counting kit-8 assay (CCK-8). LLC cells at a cell density of 5×10^3 cells per well were seeded into the 96-well plates and cultured for 24 h. Cells were co-incubated with RLDPB (dBET6 concentration, 0 ~ 10 μg/mL) for 24 h. Then, CCK-8 solution (10%) was added into each well and incubated with the treated cells for 4 h. After that, the absorbance of each well was determined at 450 nm by a microplate reader (Thermo, USA) to calculate the cell viability according to the following formula. LLC cells without RLDPB treatment were selected as the negative control.

$$\text{Cell viability}(\%) = [(\text{As} - \text{Ab})/\text{Ac} - \text{Ab}] \times 100\% \quad (4)$$

Where A_s represents the absorbance of the tested samples, A_b represents the absorbance of blank wells, and A_c represents the absorbance of the negative controls.

Live/Dead staining assay

The cytotoxicity of RLDPB was also investigated by Live/Dead staining. LLC cells with a cell density of 3×10^5 cells per well were seeded into the confocal dishes and cultured for 24 h. Then, cells were incubated with RLDP, free dBET6, DPB, LDPB, and RLDPB (dBET6 equivalent to 7.5 μg/mL) for 24 h, respectively. The Live/Dead staining kit containing calcein-AM and propidium iodide (PI) was used to stain the treated cells for 10 min, followed by the fluorescence microscopy observation CLSM (Zeiss 880, Germany). The untreated LLC cells served as the negative control.

Cell apoptosis assay

To investigate the cell apoptosis, LLC cells (cell density of 3×10^5 cells per well) were seeded into the 6-well plates and cultured for 24 h. LLC cells were incubated with different formulations including RLDP, free dBET6, DPB, LDPB, and RLDPB (dBET6 equivalent to 7.5 μg/mL) for 24 h, respectively. The Annexin V-FITC/PI apoptosis detection Kit (Thermo Fisher Scientific Inc., USA) was used to stain the treated cells for 15 min. The stained cells were collected, and their cell apoptosis rates were measured by flow cytometry with an EPICS XL FACS (Beckman, USA).

Cell colony assay

To investigate the cell colony ability, LLC cells with a cell density of 500 cells per well were cultured in the 6-well plates for 24 h. The cells were treated with different

formulations including RLDP, free dBET6, DPB, LDPB, and RLDPB (dBET6 equivalent to 7.5 μg/mL), respectively. After 24 h incubation, the treated cells were cultured with fresh culture medium for 7 d. The cells were fixed with 4% paraformaldehyde for 15 min, followed by the cell staining with 0.1% crystal violets. The cells were imaged by a camera before the cell washing.

Western blotting analysis

LLC cells were treated with different formulations including RLDP, free dBET6, DPB, LDPB, and RLDPB (dBET6 equivalent to 7.5 μg/mL), respectively. After 24 h incubation, the treated cells were collected and lysed with the RIPA buffer. The cell lysates were centrifuged for 10 min at 10 000 g at 4 °C, and the supernatant was collected to measure the protein content by the BCA protein kit (Beyotime, China). The extracted proteins (20 μg/well) were boiled in the loading buffer and separated by a 10% SDS-PAGE. Afterward, each sample was transferred to polyvinylidene fluoride membranes (PVDF), blocked the nonspecific binding with 5% skim milk, and sequentially incubated overnight with the specific antibodies as follows: Caspase 3, Cleaved Caspase 3, and BRD4 (Abcam, USA). After washing with TBST buffer thrice, the membranes were incubated with the corresponding horseradish peroxidase (HRP)-conjugated secondary antibodies (Abcam, USA) for 2 h, followed by TBST buffer wash. The protein expression signals were detected by the chemiluminescence imaging system (GE, USA). Tubulin was used as a loading control.

Circulation lifetime

The healthy C57BL/6 mice were randomly divided into 4 groups (n=3). The formulations, including DiR, DP/DiR, LDP/DiD, and RLDP/DiR (DiR equivalent to 0.75 mg/kg) were administrated to the groups, respectively. The blood was collected at 2, 4, 6, 8, 12, 24, and 48 h. After frozen-thawed thrice, the blood samples were centrifuged at 12,000 rpm for 15 min. The DiR content in the supernatant was detected by using a microplate reader (Thermo, USA).

Biodistribution by in vivo imaging

The biodistribution of RLDP was performed on the LLC tumor-bearing mice by in vivo imaging. C57BL/6 mice were subcutaneously injected with LLC cells suspension (2×10^6 cells), on the right armpits of the flanks. When the tumor reached approximately 100 mm^3, the LLC tumor-bearing mice were randomly divided into five groups as follows: saline (negative control, NC), DiR, DP/DiR, LDP/DiR, and RLDP/DiR (n=3/group). The different formulations (with the DiR dosage of 0.75 mg/kg) were intravenously injected into the LLC tumor-bearing mice via tail veins, respectively. At the predetermined time intervals (2, 4, 8, 12, 24, and 48 h), the treated mice were anesthetized with 2% isoflurane. The fluorescence images of the treated mice and their tumor tissues were captured with the near-infrared (NIR) in vivo imaging system by the excitation length of 750 nm and the emission filters of 780 nm (PerkinElmer, USA). To further investigate the biodistribution in vivo, the DiR signals in the tumors were also accessed by photoacoustic imaging (PerkinElmer, USA). After 48 h post-injection, the treated mice were sacrificed, and their major organs (including heart, liver, spleen lung, and kidney) and the dissected tumors were collected for ex vivo imaging. The fluorescence intensity was semi-quantified by the living imaging software (IVIS Lumina XRMS Series III, PerkinElmer, USA).

In vivo antitumor efficacy assessment

The in vivo antitumor efficacy of RLDPB was also investigated in the LLC tumor-bearing mouse model. The LLC tumor-bearing mice with tumor volumes of approximately 50 mm^3 were randomly divided into six groups as follows: saline (negative control, NC), RLDP, dBET6, DPB, LDPB, and RLDPB (n=5/group). The formulations were intravenously injected into the LLC tumor-bearing mice through the tail vein with the dosage of BET6 at 2.5 mg/kg every 2 days. Tumor volumes and body weights of the treated mice were measured every 2 days. The relative tumor volumes were calculated according to the formulas as follows.

$$\text{Tumor volume} = \text{LW}^2/2 \tag{5}$$

$$\text{Relative tumor volume} = \text{V}_\text{t}/\text{V}_0 \tag{6}$$

Where V_t represents the tumor volume tested during administration, and V_0 represents the initial tumor volume measured before administration.

On the 18th day, the major organs (including hearts, livers, spleens, lungs, and kidneys) and tumor tissues from the treated mice were collected. The collected tissues were fixed in 4% formalin for 24 h, then embedded with paraffin and sliced for hematoxylin-eosin (H&E) staining. To confirm the anti-apoptosis of RLDPB in tumors, the sliced tumor tissues were investigated with TdT-mediated dUTP Nick-End Labeling (TUNEL) and Ki67 staining, respectively. The nuclei of the tumor tissues were stained with Hoechst.

Statistical analysis

All experiments were performed at least three times. Data were represented as the mean value ± standard deviations (SD). The statistical significance between the two groups was measured using the unpaired Student's t-test, Double-tail Student's t-test, or Analysis

of variance (ANOVA) with Tukey's post hoc test (two or more groups) by SPSS 13.0 software (SPSS, USA), in which $^{*}P<0.05$, $^{**}P<0.01$, and $^{***}P<0.001$ were presented as statistical significances.

Results

Construction and characterization of RLDPB

The epigenetic reader BRD4 plays an important role in lung cancer progression, which has been reported as a potential therapeutic target for lung cancer treatment [32]. dBET6 is a PROTAC reagent for the selective degradation of BRD4, which induces apoptosis on lung cancer cells and is considered an attractive approach for lung cancer treatment. However, the clinical application of dBET6 is impeded by its poor solubility, low tissue specificity, and low bioavailability. The pH/GSH responsive polymer DS-PLGA was used to load dBET (DPB) by the O/W emulsion method. To optimize the loading efficiency and entrapment efficiency, DPB was prepared with different ratios of DS-PLGA to dBET6. DPB showed excellent loading efficiency (~15%) and entrapment efficiency (~85%) with a DS-PLGA/dBET6 ratio of 5:1. Thus, DPB were prepared at a DS-PLGA/dBET6 weight ratio of 5:1 for further investigation (Fig. S1). DPB was further coated by LLCM (Scheme 1), with LLCM to DPB at a weight ratio of 2 exhibited a good condition of size and polydispersity index (PDI) (Fig. S2). Thus, the LLCM camouflaged nanoparticles (LDPB) were formed.

It was demonstrated that the a_vb_3 integrin receptors were overexpressed on LLC cell membranes [6], and the peptide cRGD was a targeting ligand of a_vb_3 integrin receptor [33]. To block the a_vb_3 integrin receptor on LDPB, we used cRGD-PEG to incubate with LDPB in different cRGD/LLCM ratios. To confirm the successful blockage of a_vb_3 integrin receptor, the treated nanoparticles were incubated with the a_vb_3 antibodies. Many a_vb_3 antibodies were bound to LDPB, evidenced by the blot through the chemiluminescence imaging system (Fig. S3). After the treatment with cRGD-PEG, the binding of a_vb_3 antibodies were reduced significantly with the cRGD/LLCM ratio increasing to 2:1 and 4:1, implying that the excessive cRGD blocking the a_vb_3 integrin receptors on LLC cell membranes (Fig. S3). The blockage of a_vb_3 integrin receptors was performed with a cRGD/LLCM ratio of 2:1 for further investigation. Next, the excessive cRGD-PEG-DSPE was incubated with the cRGD-PEG-blocked nanoparticles and the resulting RLDPB was formed. FRET analysis confirmed the successful conjugation of cRGD-PEG-DSPE to the surface of nanoparticles, demonstrated by emission characteristic peak of FITC and Cy3 with the excitation of 488 nm laser (Fig. S4). The nano-PROTAC (RLDPB) was expected to possess the capability of dual targeting and bioresponsiveness.

TEM and DLS analysis indicated that DPB was spherical with a diameter of 222.3 ± 4.8 nm (PDI: 0.019), while LDPB showed core-shell nanostructure with a diameter slightly increasing to 250.5 ± 4.2 nm (PDI, 0.16) after the camouflage with LLC membrane (Fig. 1A and B). RLDPB did not show significant changes in the morphology and size (257.6 ± 7.9) with a PDI of 0.13 (Fig. 1C). The zeta potential of DPB was −17.6 ± 1.6 mV, while the one of LDPB and RLDPB were corresponding to -35.4 ± 1.0 mV and −27.1 ± 2.3 mV (Fig. S5A).

The stability of RLDPB was investigated. RLDPB showed no significant differences in size (~250 nm), PDI (~0.1), and minor changes in the zeta potential (-25~-28 mV) within 96 h (Fig. 1D and Fig. S5B), which indicated the excellent stability of RLDPB. The cumulative release analysis indicated that the release of dBET6 was increased from 15 to 40% with the pH value changed from 7.4 to 5.5 within 72 h (Fig. 1E). Meanwhile, the cumulative release of dBET6 was increased to approximately 80% with the increased GSH concentration (Fig. 1E). To investigate the GSH and pH-responsive ability, RLDPB was incubated with different concentrations of GSH (5 mM and 10 mM) at pH 7.4 or 5.5. TEM observation showed that RLDPB exposed to high concentrations of GSH and low pH were easily degraded (Fig. S6). SDS-PAGE analysis indicated that the membrane proteins in LDPB and RLDPB were similar to the ones derived from LLC cell membranes (Fig. 1F and Fig. S7), implying the successful camouflage of LLCM to DPB.

Overall, we constructed RLDPB successfully. RLDPB were well-dispersed with core-shell structure, which showed excellent drug encapsulation efficiency, drug loading capacity, and stability, exhibiting pH/GSH-responsive release of dBET6 in the intracellular simulated environment. The characterizations implied that RLDPB might be a favorable nano-PROTAC system for lung cancer therapy.

Cellular uptake and intracellular trafficking of RLDPB

We studied the cellular uptake of RLDPB in LLC cells. Considering the non-fluorescence properties of dBET6, the fluorescent dye DiD was used as a probe to track the nanoparticles. The cellular uptake of RLDP/DiD showed a dosage and time-dependent manner, reaching a plateau at the DS-PLGA dosage of 200 μg/mL after incubation for 12 h (Fig. 2A and B). CLSM and FACS analysis also confirmed the effective cellular uptake of RLDP/DiD (Fig. 2C and Fig. S8). The cellular uptake assay demonstrated that the camouflage with LLC cell membrane and further modification with cRGD improved the cellular uptake, which might be attributed to the homotypic targeting effect of LLC membranes and the specific binding by cRGD. The dual targeting effect is beneficial for the targeting delivery of PROTAC to the tumors.

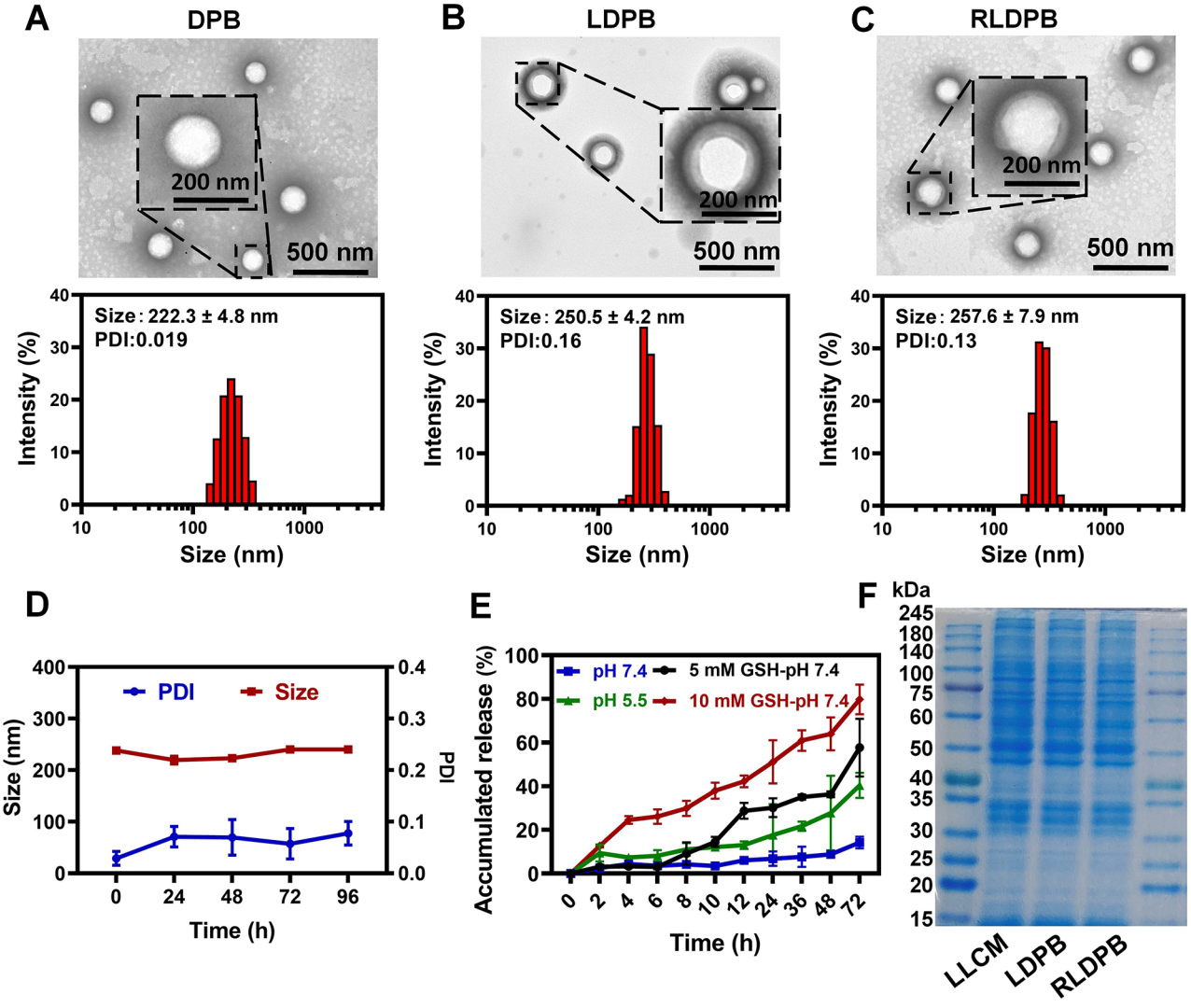

Fig. 1 Physiochemical characterizations of RLDPB. **A** TEM and DLS determination of DPB. **B** TEM observation and DLS determination of LDPB. **C** TEM and DLS determination of RLDPB. **D** Particle size determination of RLDPB by DLS within 96 h. **E** The accumulated release in different conditions (5 and 10 mM of GSH, pH 5.5, and pH 7.4) for 72 h, respectively. **F** SDS-PAGE analysis of the protein components. Lane 1, Molecular weight markers; Lane 2, LLCM, LLC cells membrane; Lane 3, LDPB; Lane 4, RLDPB; Lane 1, Molecular weight markers

Lung cancer cell inhibition induced by RLDPB

RLDPB was supposed to show effective antitumor effects on lung cancer cells. Before the study on the in vitro antitumor effect, the biocompatibility of RLDPB was evaluated. The hemolysis assay indicated that RLDPB showed no visible hemolysis within the working concentrations, indicating the excellent blood compatibility of RLDPB (Fig. 3A). Different formulations, such as PBS, RLDP, DPB, LDPB, or RLDPB also showed ignorable hemolysis (Fig. 3B). Notably, the free dBET6 showed hemolysis of ~10%, indicating the potential side effects without appropriate carriers.

Next, we investigated the in vitro cell inhibition induced by RLDPB. CCK-8 assay indicated that RLDPB showed significant cytotoxicity on LLC cells in a dBET6 dose-dependent manner (Fig. 3C), but the cell inhibition reached a plateau when the concentration of dBET6 was 7.5 μg/mL. Crystal violet staining assay indicated that the treatment with RLDPB led to the fewest colony numbers, with ~15-fold fewer than the one of PBS treated (Fig. 3D). Furthermore, Live/Dead staining assay indicated that most of the LLC cells were dead, evidenced by the emission of red fluorescence (PI positive) (Fig. 3E). The Annexin V-FITC Apoptosis Detection Kit indicated that RLDPB induced ~95% apoptosis, which indicated that most of the lung cancer cells were killed (Fig. 3F). CCK-8 assay also showed that the cell viability of LLC cells was more than 90% when the cells were exposed to RLDP without dBET6 (Fig. 3G), further confirming the effective suppressions on the cancer growth induced by RLDPB.

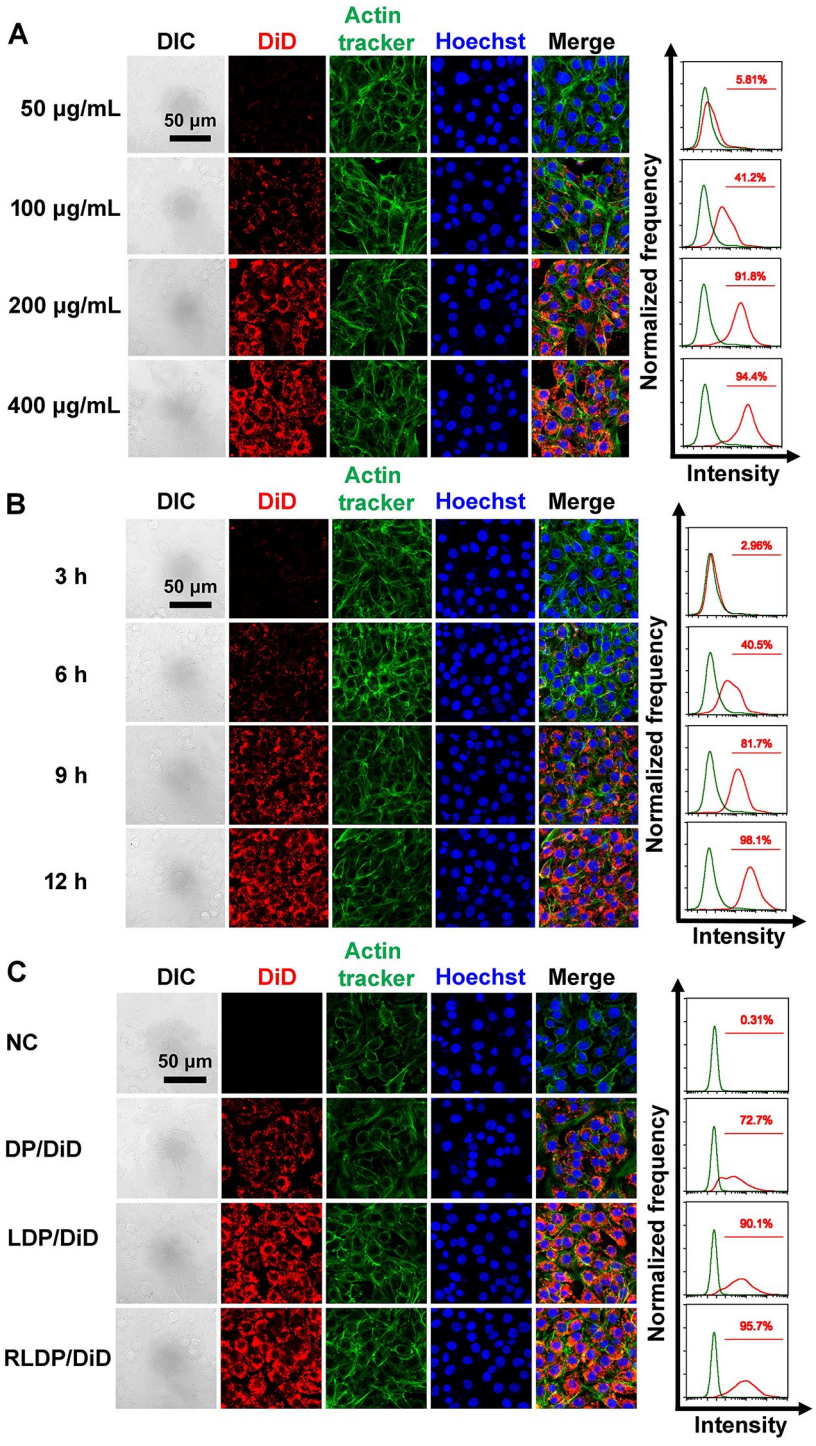

Fig. 2 CLSM and FACS analysis of the cellular uptakes of different formulations. **A** CLSM and FACS analysis of the dosage-dependent cellular uptake of RLDP/DiD. LLC cells were treated with RLDP/DiD with the DS-PLGA concentrations equivalent to 50, 100, 200, and 400 μg/mL for 12 h, respectively. **B** CLSM and FACS analysis of the time-dependent cellular uptake. LLC cells were treated with RLDP/DiD at the DS-PLGA concentration equivalent to 200 μg/mL for different incubation times (3, 6, 9, and 12 h), respectively. **C** Cellular uptake of DP/DiD, LDP/DiD, and RLDP/DiD (DS-PLGA equivalent to 200 μg/mL) for 12 h. LLC cells without any treatment served as the negative control. Excitation/Emission wavelengths were shown as follows: DiD (stained in red), 633 nm/670 nm; actin-tracker red-555 (stained in green), 555 nm/565 nm; Hoechst (stained in blue), 365 nm/420 nm

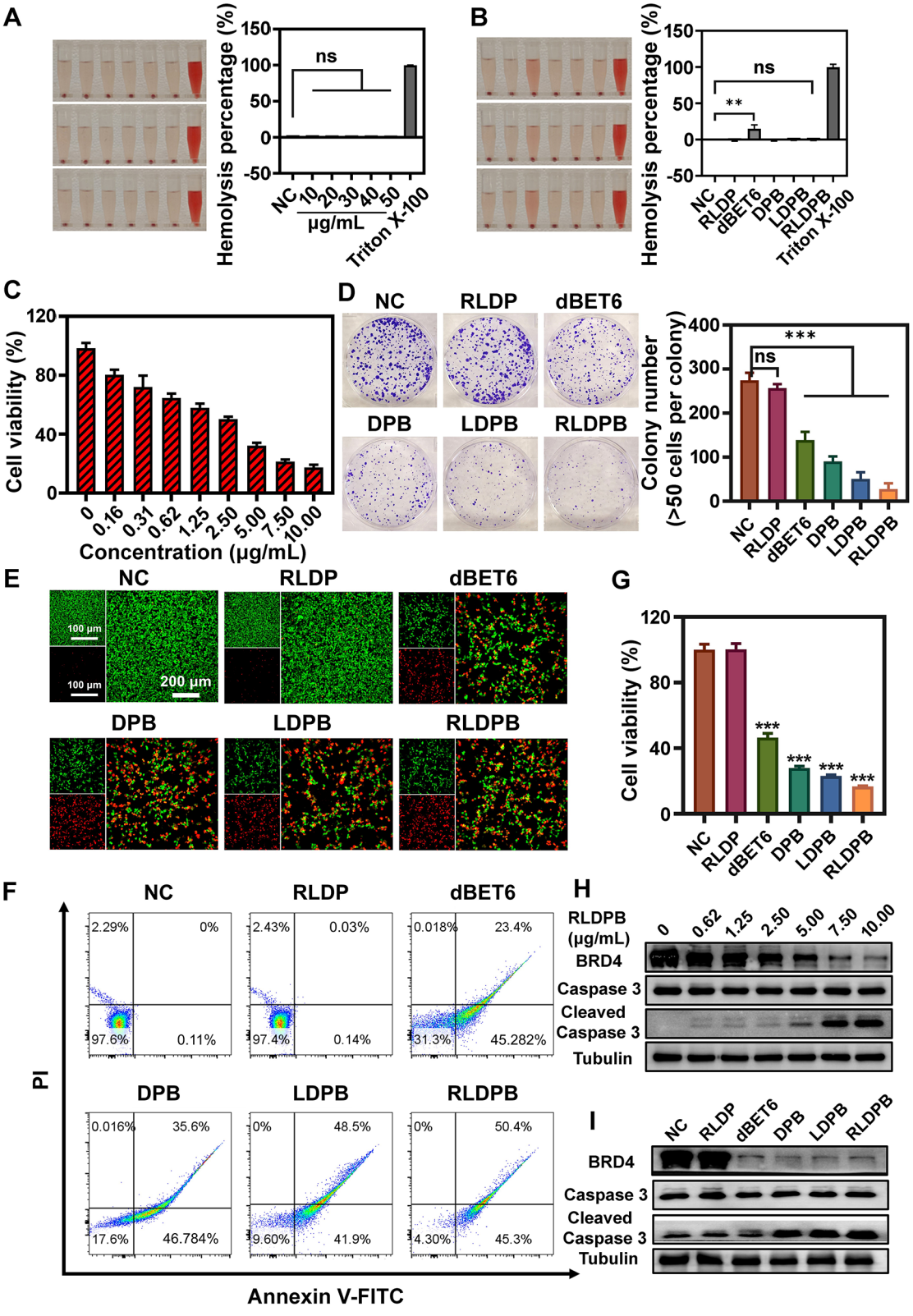

Fig. 3 (See legend on next page.)

(See figure on previous page.)

Fig. 3 In vitro lung cancer cell inhibition induced by RLDPB. **A** Hemolysis percentage of RLDPB with the dosage of dBET6 ranging from 10 to 50 μg/mL. **B** Hemolysis induced by different formulations including RLDP, free dBET6, DPB, LDPB, or RLDPB. In **A** and **B**, RBCs without any treatment served as the negative controls, while RBCs treated with 0.2% Triton X-100 were selected as the positive controls. **C** CCK-8 assay analysis of cell viability. LLC cells were treated with RLDPB in the dBET6 concentrations ranging from 0 to 10 μg/mL for 24 h. **D** The colony formation assay of different formulations including RLDP, free dBET6, DP dBET6, LDPB, and RLDPB, respectively. The colony number of RLDP, free dBET6, DPB, LDPB, and RLDPB was counted by the colony formation assay. **E** The Live/Dead staining of LLC cells treated with RLDP, free dBET6, DPB, LDPB, and RLDPB for 24 h, respectively. **F** The apoptosis induced by different formulations. LLC cells were treated with RLDP, free dBET6, DPB, LDPB, and RLDPB (dBET6 at a concentration of 7.5 μg/mL) for 24 h, followed by the Annexin V-FITC/PI staining assessed by FACS. **G** The cell viability of different formulations assessed by CCK-8. LLC cells were incubated with formulations including RLDP, free dBET6, DPB, LDPB, and RLDPB with a dBET6 concentration of 7.5 μg/mL, respectively. In C, D, E, F, and G, LLC cells without any treatments were served as the negative controls. **H** Protein levels (including BRD4, Caspase 3, and Cleaved Caspase 3) in LLC cells treated with RLDPB. LLC cells were treated with RLDPB at different dBET6 concentrations (0, 0.625, 1.25, 2.5, 5, 7.5, and 10 μg/mL) for 24 h, followed by the assessment of western blotting. **I** Protein levels (including BRD4, Caspase 3, and Cleaved Caspase 3) in LLC cells treated with different nanoparticles. LLC cells were incubated with RLDP, dBET6, DPB, LDPB, and RLDPB for 24 h, respectively, followed by the assessment of western blotting. In **H** and **I**, the expression of Tubulin was determined as a control

We further explored the mechanism of enhanced antitumor effect induced by RLDPB. dBET6 is an epigenetic reader degradation of BRD4 that is demonstrated to selectively degrade the protein BRD4 in lung cancer cells [34]. WB analysis indicated that RLDPB exhibited an effective BRD4 degradation capacity in a dBET6 dosage-dependent manner (Fig. 3H). The degradation of BRD4 induced by dBET6 led to the up-regulation of cleaved caspase 3 (Fig. 3H), which inhibited the progress and development of lung cancer. To confirm the enhanced BRD4 degradation capacity induced by RLDPB, the related protein expressions (including BRD4, Caspase 3, and Cleaved Caspase 3) in LLC cells treated with different formulations were also determined by WB analysis. As expected, dBET6-loaded formulations (including RLDPB, LDPB, DPB, and dBET6) significantly down-regulated the expression level of BRD4 (Fig. 3I). RLDPB showed the strongest BRD4 degradation ability in all the dBET6-loaded formulations.

The results suggested that RLDPB exhibited an excellent inhibition on lung cancer cells, demonstrated by the BRD4 degradation and activation of the Caspase-3-related apoptosis pathway. The enhanced antitumor effect induced by RLDPB is ascribed to the excellent performance on the dual targeting and responsive release of dBET6. On the one hand, the enhanced specificity improved the accumulation of dBET6 in the lung cancer cells; on the other hand, the pH/GSH responsiveness accelerated the release of dBET6 within the cancer cells.

In vivo biodistribution

We assessed the biodistribution and circulation lifetime of different formulations in vivo, which was important for lung cancer therapy [35]. To capture the in vivo imaging, the near-infrared (NIR) fluorescent dye DiR was used as a substitution for dBET6. In vivo biodistribution was performed on LLC tumor-bearing mice by in vivo imaging. RLDP/DiR showed the strongest fluorescence intensity in the tumor sites, compared with the other groups with 8 h post-injection and continuing to 48 h (Fig. 4A). Although the administration with DiR, DP/DiR, or LDP/DiR also showed some fluorescence in the tumor sites, the signals were significantly lower compared with the one of RLDP/DiR. The extracted major organs were also detected by the in vivo imaging system, which indicated that the administration with RLDP/DiR showed the highest fluorescence level in the tumors, compared to the groups such as DiR, DP/DiR, or LDP/DiR. Interestingly, the treatment with RLDP/DiR showed weaker DiR signals in the liver than the other groups (Fig. 4B and C). The in vivo biodistribution assay indicated that the camouflage with LLCM and further modification with cRGD improved the specificity of the tumors.

To further investigate the accumulation in tumors, the formulations were assessed on the LLC tumor-bearing mice by in vivo photoacoustic imaging. The DiR signals in the tumors were gradually increased and reached a maximum fluorescent intensity at 8 h in all the DiR-loaded formulations. Consistent with the in vivo imaging, RLDP/DiR exhibited the strongest DiR signals among the formulations (Fig. 4D and E), which might be attributed to the specificity by the homotypic targeting of LLC membranes and improved targeting effect of cRGD. The photoacoustic imaging confirmed that the camouflage with LLC membranes and further modification with cRGD improved the tumor accumulation effectively.

We also detected the circulation lifetime in vivo. After different formulations were administrated to the healthy C57BL/6, the blood concentration of RLDP/DiR was ~ 2-fold to the one of free DiR or bare DPB ranging from 10 h to 48 h, similar to the one of LDP/DiR (Fig. S9), implying that the modification with cRGD did not affect the circulation lifetime significantly. The improved circulation increased the probability of targeted delivery to the tumor tissues, avoiding the potential side effects on the healthy ones.

The in vivo imaging and photoacoustic imaging together proved that RLDP/DiR possessed excellent specific accumulation capacity on LLC tumors. Furthermore, the camouflage with LLC membranes prolonged circulation lifetime of nanoparticles. These properties of

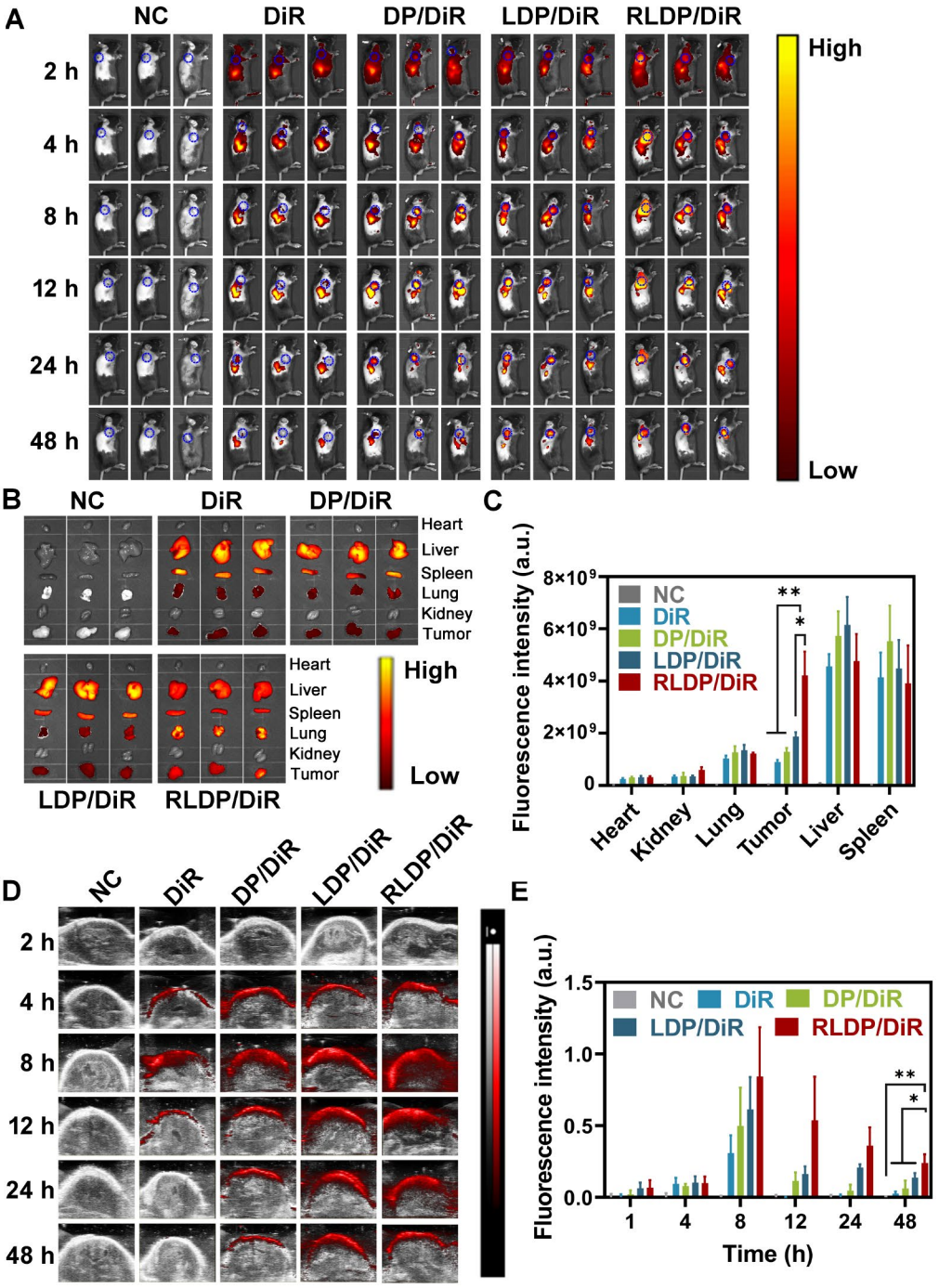

Fig. 4 The in vivo biodistribution and tumor targeting accumulations. **A** The in vivo images of different DiR labeled nanoparticles (including DiR, DP/DiR, LDP/DiR, and RLDP/DiR) in the LLC tumor-bearing mice after administration. LLC tumor-bearing mice were intravenously injected with DiR, DP/DiR, LDP/DiR, and RLDP/DiR at a DiR dosage of 0.75 mg/kg, following the in vivo imaging at a predetermined time (2, 4, 8, 12, 24, and 48 h), respectively. **B** The ex vivo imaging of different DiR-loaded nanoparticles in major tissues of the treated mice after 48 h administration. **C** The quantitative analysis of the fluorescence intensity induced by different DiR-loaded nanoparticles in the extracted major tissues. **D** The photoacoustic imaging of different DiR-labeled nanoparticles in tumors. LLC tumor-bearing mice were intravenously injected with DiR, DP/DiR, LDP/DiR, and RLDP/DiR at a DiR dosage of 0.75 mg/kg, followed by the photoacoustic images at the predetermined time (2, 4, 8, 12, 24, and 48 h), respectively. **E** The quantitative analysis of fluorescence intensity in the tumors by photoacoustic imaging. The blue circles represent the tumor sites. Data were expressed as mean ± SD ($n = 3$). *, $P < 0.05$; **, $P < 0.01$

the dual targeting nanostructures exerted efficient antitumor effects on the precise treatment of lung cancer.

The in vivo tumor suppression

To investigate the in vivo anti-tumor effects of RLDPB, LLC tumor-bearing mice were established, followed by the intravenous administration of dBET6 loaded nanoparticles every other day (Fig. 5A). As shown in Fig. 5B and C, RLDPB achieved the best tumor inhibition effect, with the tumor volumes decreasing to ~ one-fifteenth of the ones treated with saline or RLDP. The free dBET6 showed some suppression of the tumor growth but without significant differences compared with the negative controls (saline), which might be attributed to the low accumulations of dBET6 in the tumors. The dBET6-loaded nanoparticles including RLDPB, LDPB, and DPB, displayed better anti-tumor effects compared to free dBET6 (Fig. 5B and C), but inferior to the one of RLDPB. The body weight test indicated that the dBET6-loaded nanoparticles showed no significant changes in the weight of the LLC tumor-bearing mice (Fig. 5D), implying the safety of the dBET6-loaded nanoparticles. In accordance with the systemic tumor suppression, the HE, TUNEL, and Ki67 stained tumor pathological sections demonstrated that RLDPB exerted more significant tumor cell apoptosis and less Ki67 compared to the other treatments (including saline, RLDP, dBET6, DPB, and LDPB), which further demonstrated the enhanced tumor suppression on RLDPB (Fig. 5E and Fig. S10). Meanwhile, the H&E staining showed the major organs (including hearts, livers, spleens, lungs, and kidneys) showed no obvious systemic toxicity after different treatments (Fig. S11), implying the in vivo biosafety of the dBET6-loaded nanoparticles. The data indicated that RLDPB showed effective tumor inhibition in vivo, which might be attributed to the excellent performance of RLDPB including the prolonged circulation lifetime, dual targeting, and pH/GSH responsiveness. RLDPB showed great potential in the treatment of lung cancer.

Discussion

Epigenetic regulation is a promising therapeutic strategy for lung cancer treatment, which can modulate epigenetic dysregulation of the targeted read proteins in tumors to achieve tumor suppression [5, 36]. A proteolysis-targeting chimera is an effective tool for epigenetic regulation that precisely degrades targeted reader proteins in tumors with the ubiquitin-proteasome system [37, 38]. Notably, bromodomain-containing protein 4 (BRD4), a reader protein of the BET family, promotes tumor growth with apparent epigenetic dysregulation in tumors, which was considered a potential target for solid tumors [39, 40]. dBET6 is a PROTAC reagent of BRD4, which facilitates the antitumor effect by targeted degradation of BRD4 to induce cell apoptosis through the Caspase 3 activity [41]. In our present work, dBET6 was chosen as a potential epigenetic degradation agent to achieve tumor suppression for lung cancer therapy. Compared with conventional chemotherapy, dBET6 shows great potential in lung cancer treatment due to its effective epigenetic protein degradation effect [29]. However, the low bioavailability and tissue specificity of this type of PROTAC regent limited its applications in lung cancer therapy.

Biomimetic nanotechnology endowed the nanoparticles with improved surface functions, which significantly enhanced the stability and antitumor effect for lung cancer treatment [42]. Herein, to improve the specificity and bioavailability, the PROTAC agent dBET6 was loaded onto the biodegradable DS-PLGA nanoparticles, followed by the camouflage with LLC cell membranes and further modified with cRGD as the dual targeting and bioresponsive drug delivery system.

As expected, the bioinspired nano-PROTAC system (RLDPB) was demonstrated to possess a prolonged circulation lifetime and also display excellent homologous targeting by the camouflage with LLC membranes, as well as the active targeting ability by the specific binding of avb3 integrin receptors with cRGD. However, the tumor microenvironment is complicated, consisting of cancer cells, immune cells, fibroblasts, and so forth. RLDPB may also be uptaken by these cells, and affect the cell conditions. In the present study, RLDPB was constructed with the homotypic cell membranes and cRGD to maximize the specificity of the lung cancer cells, which induced effective apoptosis and inhibition of the proliferation in the tumor tissues, and led to the suppression of tumor growth (Fig. 5). The enhanced accumulations of dBET6 in tumors facilitated the significant tumor regression. These findings provided a novel strategy for the targeted delivery of PROTAC for lung cancer treatment.

Drug release plays an important role in lung cancer therapy. The antitumor effect cannot be achieved in cells unless the drugs are released from the nanoparticles. Stimuli-responsive nanoparticles triggered drug release in tumor cells with different endogenous stimuli based on the cellular environments [43]. The acidic environment in the lysosome and high-level expression of glutathione (GSH) exist in the lung cancer cells, which are important conditions for designing the drug delivery systems and are available for lung cancer therapy. In this work, the disulfide-linkage PLGA (DSP) was utilized to load dBET6. It was proved that the dBET6-containing structure showed stimuli-responsive drug release because the cleavable ester bond and -S-S bond were triggered by the acidic pH and high GSH level within the cells. Notably, the tumor microenvironment usually possesses acidic pH and high GSH conditions. The cargo-loaded nanoparticles benefited from the good protection of cell

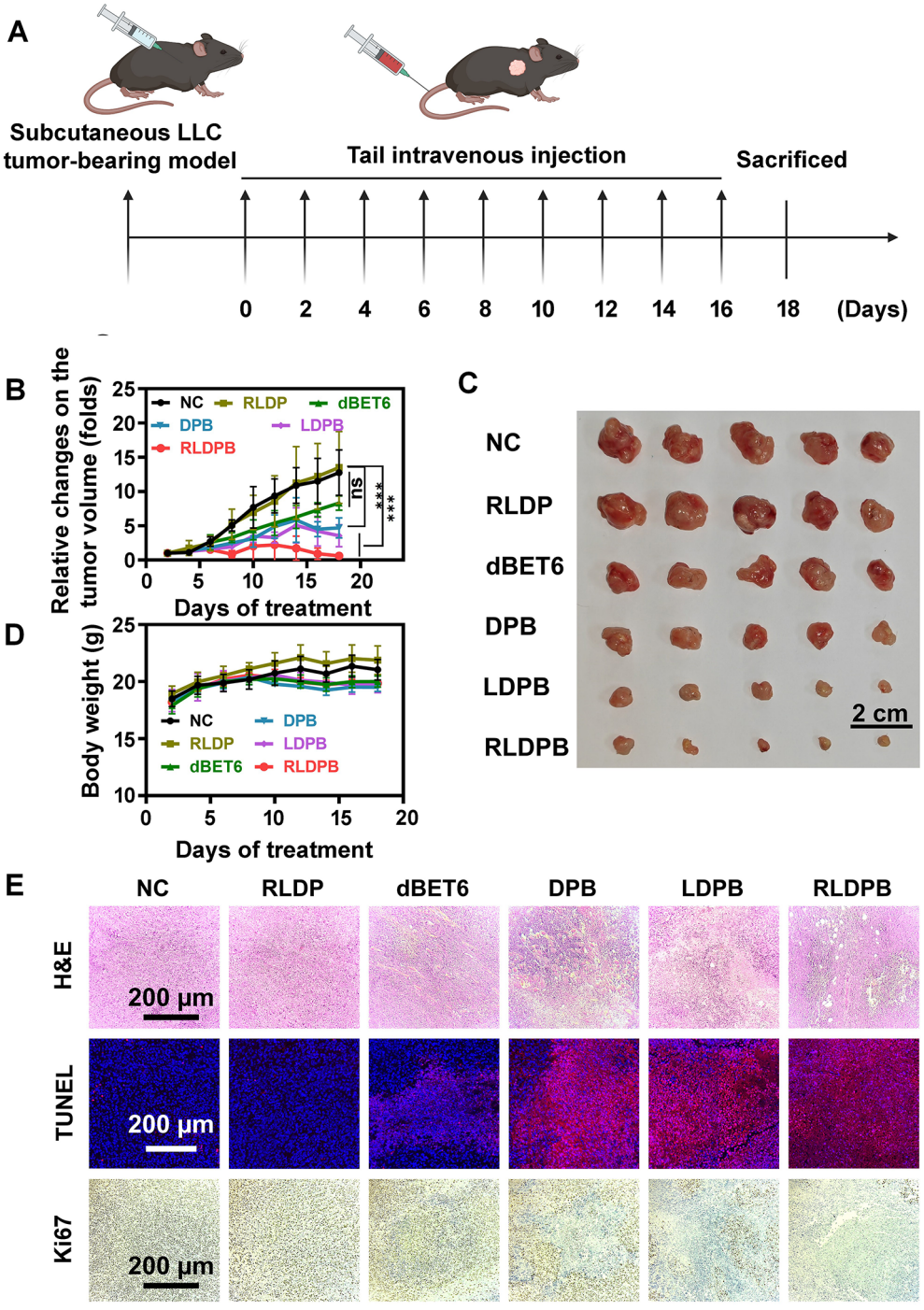

Fig. 5 The in vivo anti-tumor effect of dBET6 loaded nanoparticles on LLC tumor-bearing mice. **A** Schematic illustration of the intravenous treatment with dBET6-containing formulations in the LLC tumor-bearing mice. **B** The relative tumor volumes of the treated LLC tumor-bearing mice during the treatment period. LLC tumor-bearing mice were intravenously injected with formulations including saline, RLDP, dBET6, DPB, LDPB, and RLDPB, followed by the detection for the relative tumor volumes, respectively. **C** Photographs of tumors collected from the LLC tumor-bearing mice after different treatments for 18 days. **D** Body weight of the treated LLC tumor-bearing mice during the treatment period. **E** HE, TUNEL, and Ki67 staining images of tumor sections after different treatments. The LLC tumor-bearing mice were treated with formulations including saline, RLDP, dBET6, DPB, LDPB, and RLDPB, respectively. Then, tumors were collected from the treated mice, followed by the staining of HE, TUNEL, and Ki67, respectively. $n = 5$, mean ± SD. ***, $P < 0.001$

membranes, which avoided preliminary exposure to the tumor microenvironments. Overall, these findings demonstrated that RLDPB displayed enhanced tumor inhibition with the pH/GSH responsiveness, which provided a potential tool for the epigenetic reader degradation in lung cancer treatment.

Conclusion

In conclusion, we successfully developed a type of dual targeting and bioresponsive nano-PROTAC (RLDPB), which was constructed by using the pH/GSH- -responsive polymer DS-PLGA to load the PROTAC agent dBET6, and further camouflaged with LLC membrane and modified with cRGD. RLDPB exhibited excellent drug loading capacity, biodegradable ability, and pH/GSH responsive release behavior. RLDPB possessed a dual targeting effect based on the homotypic and active targeting ability and enhanced cellular uptake was achieved. The pH and GSH responsive capacity accelerated the intracellular release of dBET6, which resulted in the effective apoptosis of lung cancer cells by degrading the epigenetic reader BRD4. The dual targeting and bioresponsive nano-PROTAC showed enhanced tumor inhibition through the Caspase-3 pathway induced by the downregulation of BRD4. Therefore, RLDPB was a potential bioinspired nano-PROTAC system that can be applied to the precise treatment of lung cancer.

Supplementary Information

The online version contains supplementary material available at https://doi.org/10.1186/s12951-024-02967-7.

Supplementary Material 1

Acknowledgements
Not applicable.

Author contributions
XG, XX, and YT carried out the experiments, data collection, and data analysis. XD, LH, ZL, JC, JH, and DZ performed the methodology and verification. LZ and XY performed on the conceptualization, supervision, and writing review. LZ and MW wrote the original draft, and performed the review, and editing. All authors read and approved the final manuscript.

Funding
This work was financially supported by the National Key Research and Development Program of China (2022YFE0209700), National Natural Science Foundation of China (82072047 and 32171312), Research Foundation of Education Bureau of Guangdong Province (2021ZDZX2004), the Guangzhou Science and Technology Project (2024A03J0891, 202201011593, and SL2022A03J00613), Plan on enhancing scientific research in GMU (02-410-2302068XM), The Open research funds from The Sixth Affiliated Hospital of Guangzhou Medical University, Qingyuan Peoples Hospital (202201-303).

Data availability
No datasets were generated or analysed during the current study.

Declarations

Ethics approval and consent to participate
Animal experiments were permitted by the Institutional Animal Care and Use Committee (No. S2023-770) and performed under the guidelines of the Animal Welfare Act of Guangzhou Medical University.

Consent for publication
Not applicable.

Competing interests
The authors declare no competing interests.

Author details
[1]The Fifth Affiliated Hospital, The Affiliated Panyu Central Hospital, Guangzhou Municipal and Guangdong Provincial Key Laboratory of Molecular Target & Clinical Pharmacology, The NMPA and State Key Laboratory of Respiratory Disease, The School of Pharmaceutical Sciences, Guangzhou Medical University, Guangzhou, Guangdong 511436, China
[2]Department of Cardiology, The Third Affiliated Hospital of Guangzhou Medical University, Guangzhou 510150, China
[3]State Key Laboratory of Respiratory Disease, National Clinical Research Center for Respiratory Disease, National Center for Respiratory Medicine, Guangzhou Institute of Respiratory Health, The First Affiliated Hospital of Guangzhou Medical University, Guangzhou 510120, China

Received: 22 April 2024 / Accepted: 3 November 2024
Published online: 10 November 2024

References

1. Siegel RL, Giaquinto AN, Jemal A. Cancer statistics, 2024. CA Cancer J Clin. 2024;74:12–49.
2. Hirsch FR, Scagliotti GV, Mulshine JL, Kwon R, Curran WJ, Wu YL, et al. Lung cancer: current therapies and new targeted treatments. Lancet. 2017;389:299–311.
3. Chaft JE, Rimner A, Weder W, Azzoli CG, Kris MG, Cascone T. Evolution of systemic therapy for stages I-III non-metastatic non-small-cell lung cancer. Nat Rev Clin Oncol. 2021;18:547–57.
4. Zhang L, Lin Y, Li S, Guan X, Jiang X. In situ reprogramming of tumor-associated macrophages with internally and externally engineered exosomes. Angew Chem Int Ed. 2023;62:e202217089.
5. Jones PA, Ohtani H, Chakravarthy A, De Carvalho DD. Epigenetic therapy in immune-oncology. Nat Rev Cancer. 2019;19:151–61.
6. Li H, Li H, Li S, Li S, Lin Y, Lin Y, et al. Artificial exosomes mediated spatiotemporal-resolved and targeted delivery of epigenetic inhibitors. J Nanobiotechnol. 2021;19:364.
7. Jin W, Tan H, Wu J, He G, Liu B. Dual-target inhibitors of bromodomain-containing protein 4 (BRD4) in cancer therapy: current situation and future directions. Drug Discov Today. 2022;27:246–56.
8. Cochran AG, Conery AR, Sims RJ III. Bromodomains: a new target class for drug development. Nat Rev Drug Discov. 2019;18:609–28.
9. Nieto-Jimenez C, Galan-Moya EM, Corrales-Sanchez V, del Noblejas-Lopez M, Burgos M, Domingo M. Inhibition of the mitotic kinase PLK1 overcomes therapeutic resistance to BET inhibitors in triple negative breast cancer. Cancer Lett. 2020;491:50–9.
10. Wang Y, Jiang X, Feng F, Liu W, Sun H. Degradation of proteins by PROTACs and other strategies. Acta Pharm Sin B. 2020;10:207–38.
11. Chirnomas D, Hornberger KR, Crews CM. Protein degraders enter the clinic-a new approach to cancer therapy. Nat Rev Clin Oncol. 2023;20:265–78.
12. Zong D, Gu J, Cavalcante GC, Yao W, Zhang G, Wang S, et al. BRD4 levels determine the response of human lung cancer cells to BET degraders that potently induce apoptosis through suppression of Mcl-1. Cancer Res. 2020;80:2380–93.
13. Huang J, Yao Z, Li B, Ping Y. Targeted delivery of PROTAC-based prodrug activated by bond-cleavage bioorthogonal chemistry for microneedle-assisted cancer therapy. J Controlled Release. 2023;361:270–9.
14. He SP, Fang YX, Zhu YJ, Ma ZY, Dong GQ, Sheng CQ. Drugtamer-PROTAC conjugation strategy for targeted PROTAC delivery and synergistic antitumor therapy. Adv Sci. 2024;11:2401623.

15. Teng XC, Zhao X, Dai YC, Zhang XD, Zhang QS, Wu YC, et al. ClickRNA-PROTAC for tumor-selective protein degradation and targeted cancer therapy. J Am Chem Soc. 2024;146:27382–91.
16. Gao J, Hou B, Zhu QW, Yang L, Jiang XY, Zou ZF, et al. Engineered bioorthogonal POLY-PROTAC nanoparticles for tumour-specific protein degradation and precise cancer therapy. Nat Commun. 2022;13:4318.
17. Zhang C, Zeng ZL, Cui D, He SS, Jiang YY, Li JC, et al. Semiconducting polymer nano-PROTACs for activatable photo-immunometabolic cancer therapy. Nat Commun. 2021;12:2934.
18. Zhang W, Jin Y, Wang J, Gu M, Wang Y, Zhang X, et al. Co-delivery of PROTAC and siRNA via novel liposomes for the treatment of malignant tumors. J Colloid Interface Sci. 2025;678:896–907.
19. Fang RH, Kroll AV, Gao W, Zhang L. Cell membrane coating nanotechnology. Adv Mater. 2018;30:e1706759.
20. Lin Y, Guan X, Su J, Chen S, Fu X, Xu X, et al. Cell membrane-camouflaged nanoparticles mediated nucleic acids delivery. Int J Nanomed. 2023;18:8001–21.
21. Chen M, Sun Y, Liu H. Cell membrane biomimetic nanomedicines for cancer phototherapy. Interdiscip Med. 2023;1:e20220012.
22. Zhang Y, Yang L, Wang H, Huang J, Lin Y, Chen S, et al. Bioinspired metal-organic frameworks mediated efficient delivery of siRNA for cancer therapy. Chem Engin J. 2021;426:131926.
23. Li H, Peng Q, Yang L, Lin Y, Chen S, Qin Y, et al. High-performance dual combination therapy for cancer treatment with hybrid membrane-camouflaged mesoporous silica gold nanorods. ACS Appl Mater Interfaces. 2020;12:57732–45.
24. Zhang L, Deng S, Zhang Y, Peng Q, Li H, Wang P, et al. Homotypic targeting delivery of siRNA with artificial cancer cells. Adv Healthc Mater. 2020;9:e1900772.
25. Chen L, Hong W, Ren W, Xu T, Qian Z, He Z. Recent progress in targeted delivery vectors based on biomimetic nanoparticles. Signal Transduct Target Ther. 2021;6:225.
26. Wen Q, Zhang Y, Muluh TA, Xiong K, Wang B, Lu Y, et al. Erythrocyte membrane-camouflaged gefitinib/albumin nanoparticles for tumor imaging and targeted therapy against lung cancer. Int J Biol Macromol. 2021;193:228–37.
27. Panyam J, Labhasetwar V. Dynamics of endocytosis and exocytosis of poly(D,L-Lactide-co-Glycolide) nanoparticles in vascular smooth muscle cells. Pharm Res. 2003;20:212–20.
28. Xu E, Saltzman WM, Piotrowski-Daspit AS. Escaping the endosome: assessing cellular trafficking mechanisms of non-viral vehicles. J Controlled Release. 2021;335:465–80.
29. Zhang HT, Peng R, Chen S, Shen A, Zhao L, Tang W, et al. Versatile nano-PROTAC-induced epigenetic reader degradation for efficient lung cancer therapy. Adv Sci. 2022;9:e2202039.
30. Dong Y, Xia P, Xu X, Shen J, Ding Y, Jiang Y, et al. Targeted delivery of organic small-molecule photothermal materials with engineered extracellular vesicles for imaging-guided tumor photothermal therapy. J Nanobiotechnol. 2023;21:442.
31. Qin A, Chen S, Li S, Li Q, Huang X, Xia L, et al. Artificial stem cells mediated inflammation-tropic delivery of antiviral drugs for pneumonia treatment. J Nanobiotechnol. 2022;20:335.
32. Donati B, Lorenzini E, Ciarrocchi A. BRD4 and Cancer: going beyond transcriptional regulation. Mol Cancer. 2019;17:164.
33. Hao Y, Li H, Ge X, Liu Y, Li X, Liu Y, et al. Tumor-selective activation of toll-like receptor 7/8 agonist nano-immunomodulator generates safe anti-tumor immune responses upon systemic administration. Angew Chem Int Ed. 2022;61:e202214992.
34. Nabet B, Ferguson FM, Seong BKA, Kuljanin M, Leggett AL, Mohardt ML, et al. Rapid and direct control of target protein levels with VHL-recruiting dTAG molecules. Nat Commun. 2020;11:4687.
35. Liang L, Cen H, Huang J, Qin A, Xu W, Wang S, et al. The reversion of DNA methylation-induced miRNA silence via biomimetic nanoparticles-mediated gene delivery for efficient lung adenocarcinoma therapy. Mol Cancer. 2022;21:186.
36. Peng Q, Li H, Deng Q, Liang L, Wang F, Lin Y, et al. Hybrid artificial cell-mediated epigenetic inhibition in metastatic lung cancer. J Colloid Interface Sci. 2021;603:319–32.
37. Burslem GM, Crews CM. Proteolysis-targeting chimeras as therapeutics and tools for biological discovery. Cell. 2020;181:102–14.
38. Gao J, Yang L, Lei SM, Zhou F, Nie HJ, Peng B, et al. Stimuli-activatable PROTACs for precise protein degradation and cancer therapy. Sci Bull. 2023;68:1069–85.
39. Zhao X, Chen Y, Su H, Zhang L. From classic medicinal chemistry to state-of-the-art interdisciplinary medicine: recent advances in proteolysis-targeting chimeras technology. Interdiscip Med. 2023;1:e20230004.
40. Yang T, Hu Y, Miao J, Chen J, Liu J, Cheng Y, et al. A BRD4 PROTAC nanodrug for glioma therapy *via* the intervention of tumor cells proliferation, apoptosis and M2 macrophages polarization. Acta Pharm Sin B. 2022;12:2658–71.
41. Mori Y, Akizuki Y, Honda R, Takao M, Tsuchimoto A, Hashimoto S, et al. Intrinsic signaling pathways modulate targeted protein degradation. Nat Commun. 2024;15:5379.
42. Lin Y, Yi M, Guan X, Chen E, Yang L, Li S, et al. Two birds with one stone strategy for the lung cancer therapy with bioinspired AIE aggregates. J Nanobiotechnol. 2023;21:49.
43. Mi P. Stimuli-responsive nanocarriers for drug delivery, tumor imaging, therapy and theranostics. Theranostics. 2020;10:4557–88.

Publisher's note